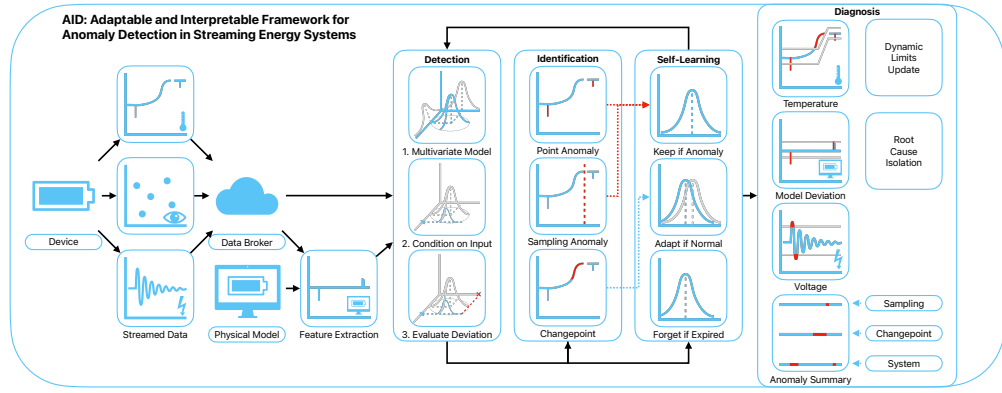


# Graphical Abstract

## Adaptable and Interpretable Framework for Anomaly Detection in SCADA-based IoT Systems

Marek Wadinger, Michal Kvasnica



## Highlights

### **Adaptable and Interpretable Framework for Anomaly Detection in SCADA-based IoT Systems**

Marek Wadinger, Michal Kvasnica

- First interpretable anomaly detector with self-supervised adaptation
- Delivers comparable performance to established general methods
- Isolates root cause of anomalies while considering interactions
- Demonstrates interpretability by providing process limits for signals
- Uses self-learning approach on streamed IoT data

# Adaptable and Interpretable Framework for Anomaly Detection in SCADA-based IoT Systems

Marek Wadinger<sup>a,b</sup>, Michal Kvasnica<sup>a,b</sup>

<sup>a</sup>*Institute of Information Engineering, Automation and Mathematics, Slovak University of Technology in Bratislava,*

<sup>b</sup>*Tesla 50Hz s.r.o.,*

---

## Abstract

In this paper, we introduce an Adaptable and Interpretable Framework for Anomaly Detection (AID) designed for industrial systems utilizing IoT data streams on top of well-established SCADA systems. AID leverages dynamic conditional probability distribution modeling to capture the normal operation of dynamic systems and isolate the root causes of anomalies. The self-supervised framework dynamically updates parameters of underlying model, allowing it to adapt to non-stationarity. AID interprets anomalies as significant deviations from conditional probability, encompassing interactions as well as both spatial and temporal irregularities by exposing them as features. Crucially, AID provides dynamic process limits to integrate with existing alarm handling mechanisms in SCADA and pinpoint root causes at the level of individual inputs. Two industrial-scale case studies showcase AID’s capabilities. The first study showcases AID’s effectiveness on energy storage system, adapting to changes, setting less conservative process limits for SCADA, and ability to leverage a physical model. The second study monitors battery module temperatures, where AID identifies hardware faults, emphasizing its relevance to energy storage safety. A benchmark evaluation on real data shows that AID delivers comparable performance to other self-learning adaptable anomaly detection methods, with the significant advancement in diagnostic capabilities for improved system reliability and performance.

*Keywords:* Anomaly detection, Root cause isolation, Iterative learning, Statistical learning, Self-supervised learning

---

*Email address:* `marek.wadinger@stuba.sk` (Marek Wadinger)  
*URL:* `uiam.sk/~wadinger` (Marek Wadinger)

---

## <sup>1</sup> 1. Introduction

<sup>2</sup> Anomaly detection systems play a critical role in risk-averse systems by  
<sup>3</sup> identifying abnormal patterns and adapting to novel expected patterns in  
<sup>4</sup> data. These systems are particularly vital in the context of Internet of Things  
<sup>5</sup> (IoT) devices that continuously stream high-fidelity data to control units.

<sup>6</sup> In this rapidly evolving field with long-spanning roots, Chandola et al.  
<sup>7</sup> conducted an influential review of prior research efforts across diverse appli-  
<sup>8</sup> cation domains (Chandola et al. (2009)). Recent studies have underscored  
<sup>9</sup> the need for holistic and tunable anomaly detection methods accessible to  
<sup>10</sup> operators (Laptev et al. (2015); Kejariwal (2015); Cook et al. (2020)).

<sup>11</sup> Cook et al. denote substantial aspects that pose challenges to anomaly  
<sup>12</sup> detection in IoT, including the temporal, spatial, and external context of  
<sup>13</sup> measurements, multivariate characteristics, noise, and nonstationarity (Cook  
<sup>14</sup> et al. (2020)). To address these complexity issues, Zhang et al. have suc-  
<sup>15</sup> cessfully employed spatially distributed sensors and time-relative modula-  
<sup>16</sup> tion. Their approach has proven effective, particularly in the context of com-  
<sup>17</sup> plex non-linear systems, offering potential solutions to some of the challenges  
<sup>18</sup> posed by IoT data (Zhang et al. (2024)). Huang et al., on the other hand,  
<sup>19</sup> tackled the problems of detecting global outliers, local outliers, and outlier  
<sup>20</sup> clusters simultaneously. Their proposed approach, based on density estima-  
<sup>21</sup> tion, relies on the notion that density distributions should exhibit minimal  
<sup>22</sup> variations in local areas. To achieve this, they introduce a novel turning ra-  
<sup>23</sup> tio metric, which reduces reliance on hyperparameters and enhances anomaly  
<sup>24</sup> detection (Huang et al. (2023)).

<sup>25</sup> Additionally, feature engineering techniques play a crucial role in cap-  
<sup>26</sup> turing contextual properties and enhancing anomaly detection performance  
<sup>27</sup> (Fan et al. (2019)). However, it is worth noting that feature engineering  
<sup>28</sup> may introduce categorical variables and significantly increase the dimen-  
<sup>29</sup> sionality of the data, requiring specific methods for handling large data, size-  
<sup>30</sup> able data storage, and substantial computational resources (Talagala et al.  
<sup>31</sup> (2021)). Recently, Li et al. introduced an attribute-weighted outlier de-  
<sup>32</sup>tection algorithm, designed for high-dimensional datasets with mixtures of  
<sup>33</sup> categorical and numerical data. Their approach assigns different weights to  
<sup>34</sup> individual attributes based on their importance in anomaly detection and  
<sup>35</sup> uses these weights to calculate distances between data points. Notably, Li et

al. demonstrated the superior performance of their algorithm compared to state-of-the-art methods (Li and Liu (2024)). Another strategy for handling high-dimensional data involves using deep learning methods with synthetic normal data to enhance the detection of outliers with subtle deviations, as proposed in Du et al. (2024).

Nevertheless, the presence of nonstationarity, often stemming from concept drift (a shift in data patterns due to changes in statistical distribution) and change points (permanent alterations in system state), presents a substantial challenge (Salehi and Rashidi (2018)). In practical scenarios, those changes tend to be unpredictable in both their spatial and temporal aspects. Consequently, they require systems with solid outlier rejection capabilities of intelligent tracking algorithms (Barbosa Roa et al. (2019)). This underscores the critical importance of an anomaly detection method’s ability to adapt to evolving data structures, especially in long-term deployments. Nevertheless, as (Tartakovsky et al. (2013)) remarked, immediate detection is not a feasible option unless there is a high tolerance for false alarms.

The adaptation of batch models at scale introduces a significant latency in detector adaptation (Wu et al. (2021)). Incremental learning methods allowed adaptation while restraining the storage of the whole dataset. The supervised operator-in-the-loop solution offered by Pannu et al. showed the detector’s adaptation to data labeled on the fly (Pannu et al. (2012)). Others approached the problem as sequential processing of bounded data buffers in univariate signals (Ahmad et al. (2017)) and multivariate systems (Bosman et al. (2015)).

### 1.1. Related Work

Recent advances in anomaly detection have broadened its scope to include root cause identification governed by the development of explanatory methods capable of diagnosing and tracking faults across the system. Studies can be split into two groups of distinct approaches. The first group approaches explainability as the importance of individual features (Carletti et al. (2019); Nguyen et al. (2019); Amarasinghe et al. (2018)). Those studies allow an explanation of novelty by considering features independently. The second group uses statistical learning creating models explainable via probability. For instance, the integration of variational Bayesian inference probabilistic graph neural network allowed Zhang et al. to model the posterior distribution of sensor dependency for gas leakage localization on unlabeled data (Zhang et al.

72 (2023)). Yang et al. recently proposed a Bayesian network (BN) for fault de-  
73 tection and diagnosis. In this BN, individual nodes of the network represent  
74 normally distributed variables, whereas the multiple regression model defines  
75 weights and relationships. Using the predefined structure of the BN, the au-  
76 thors propose offline training with online detection and diagnosis (Yang et al.  
77 (2022)).

78 Given the infrequent occurrence of anomalies and their potential absence  
79 in training data, the incorporation of synthetic data or feature extraction for  
80 various detected events emerges to assist diagnosis of the system. Brito et al.  
81 designed synthetic faults based on expert knowledge and introduced them  
82 into a transfer learning classifier to exploit faults in rotating machinery, with  
83 a subsequent explanation layer (Brito et al. (2023)). Conversely, We et al.  
84 leveraged feature selection to expose various types of abnormal behavior. The  
85 team presents competitive performance while using change in relationships  
86 to provide causal inference (Wu et al. (2024)).

87 However, it is crucial to underscore that offline training, as previously em-  
88 phasized, is inherently inadequate when it comes to adapting to anticipated  
89 novel patterns, rendering it unsuitable for sustained, long-term operation on  
90 IoT devices.

91 This paper emphasizes the importance of combining adaptability in in-  
92 terpretable anomaly detection and proposes a method that addresses this  
93 challenge in real industrial systems. Here we report the discovery and char-  
94 acterization of an adaptive anomaly detection method for existing SCADA  
95 systems, employing streaming IoT data. The ability to diagnose multivariate  
96 data while providing root cause isolation via statistical learning, extends our  
97 previous contribution to the field as presented in (Wadinger and Kvasnica  
98 (2023)). The proposed algorithm represents a general method that aids a  
99 range of existing safety-critical systems where anomaly diagnosis and identi-  
100 fication are paramount.

### 101 *1.2. Novelty of proposed approach*

102 The idea of using statistical outlier detection is well-established. We  
103 highlight the impactful contributions of Yamanishi et al. in (Yamanishi and  
104 Takeuchi (2002); Yamanishi et al. (2004)). The authors propose a method for  
105 detecting anomalies in a time series. The method is based on the assumption  
106 that the continuous data is generated by a mixture of Gaussian distributions,  
107 while discrete data is modeled as histogram density. The authors solve the

108 problem of change point detection as well. However, the adaptation sys-  
109 tem is unaware of such changes, making the moving window the only source  
110 of adaptation. Our self-supervised approach facilitates intelligent adaptation  
111 concerning detected change points, to increase the speed of adaptation where  
112 the probability of concept drift is high. By leveraging its ability to adapt to  
113 changes in operational states, our proposed method operates autonomously  
114 when such changes occur. Moreover, Yamanishi et al. (2004) does not at-  
115 tempt to isolate the root cause of the anomaly. Our approach extends statis-  
116 tical outlier detection by incorporating interpretability. This is achieved by  
117 evaluating the inverse cumulative distribution function of the latest condi-  
118 tional probabilities for each measurement, considering the remainder of the  
119 measurements, and establishing limits that define the threshold for normal  
120 event probabilities.

121 A limited number of studies have focused on adaptation and interpretabil-  
122 ity within the framework of anomaly detection. Two recent contributions in  
123 this area are made by Steenwinckel et al. as reported in (Steenwinckel (2018);  
124 Steenwinckel et al. (2021)). In Steenwinckel (2018), the authors emphasize  
125 the importance of combining prior knowledge with a data-driven approach to  
126 achieve interpretability, particularly concerning root cause isolation. They  
127 propose a novel approach that involves extracting features based on knowl-  
128 edge graph pattern extraction and integrating them into the anomaly de-  
129 tection mechanism. This graph is subsequently transformed into a matrix,  
130 and adaptive region-of-interest extraction is performed using reinforcement  
131 learning techniques. To enhance interpretability, a Generative Adversarial  
132 Network (GAN) reconstructs a new graphical representation based on se-  
133 lected vectors. However, it is important to note that the validation of this  
134 idealized approach is pending further investigation. Lately, Steenwinckel  
135 et al. (2021) introduced a comprehensive framework for adaptive anomaly  
136 detection and root cause analysis in data streams. While the adaptation  
137 process is driven by user feedback, the specific mechanism remains undis-  
138 closed. The authors present an interpretation of their method through a user  
139 dashboard, featuring visualizations of raw data. This dashboard is capable of  
140 distinguishing between track-related problems and train-related issues, based  
141 on whether multiple trains at the same geographical location approach the  
142 anomaly. Meanwhile, our efforts are directed towards the development of a  
143 self-supervised method that can learn autonomously, reducing the reliance  
144 on human supervision, which is often constrained by time limitations and can  
145 lead to significant delays in adaptation. Our method is distinguished by its

146 straightforward statistical reasoning and the ability to isolate the root cause  
147 of anomalies. The interpretability of our method is demonstrated through  
148 the establishment of dynamic process limits for each signal, leveraging condi-  
149 tional probabilities derived from the signal and other system measurements  
150 and features. This provides operators with a clear understanding of the sys-  
151 tem’s state and the underlying causes of anomalies and aids existing alarm  
152 handling mechanisms in SCADA which utilize process limits. To the best  
153 of our knowledge, this study appears to be one of the initial attempts to in-  
154 troduce a self-supervised approach for adaptive anomaly detection and root  
155 cause isolation in SCADA-based systems utilizing IoT data streams.

### 156 *1.3. Broader Impact*

157 Potential applications of the proposed method are in the field of energy  
158 storage systems, where the ability to detect anomalies and isolate their root  
159 causes while adapting to changes in operation and environment, is crucial  
160 for the system safety. The proposed method is designed to be integrated  
161 into the existing infrastructure of the systems, utilizing IoT data streams on  
162 top of well-established SCADA systems. SCADA systems continuously mon-  
163 itor these process data in real-time, embodying alarm handling mechanisms,  
164 which are designed to notify operators of the system’s abnormal behavior  
165 and drive attention to the root of the problem. By comparing the current  
166 values to the upper and lower process limits, they take action when a vari-  
167 able exceeds or falls below these limits. However, safe operating limits are  
168 often established based on a combination of equipment design limits and the  
169 dynamics of the process (Stauffer and Chastain-Knight (2021)). Those are in-  
170 different to the actual state of the system and environmental conditions. The  
171 proposed method allows the establishment of dynamic process limits, which  
172 are based on the current state of the system and its environment. This allows  
173 the system to operate closer or further from its design limits, increasing its  
174 safety and profitability. The dynamic process limits allow operational metrics  
175 monitoring, making potential early detection and prevention easier. Using  
176 adaptable methods without interpretability, on the other hand, may pose  
177 safety risks and lower total financial benefits, as the triggered false alarms  
178 may need to be thoroughly analyzed, resulting in prolonged downtimes.

### 179 *1.4. Validation*

180 Two case studies show that our proposed method has the capacity to  
181 explain anomalies, isolate the root cause, and allow adaptation to change

points, advancing recently developed anomaly detection techniques for long-term deployment and cross-domain usage. We observe similar detection performance, albeit with lower scalability, on benchmark data when comparing our approach to well-established unsupervised anomaly detection methods in streamed data which create a bedrock for many state-of-the-art contributions, such as One-Class SVM (Amer et al. (2013); Liu et al. (2014); Krawczyk and Woźniak (2015); Miao et al. (2019); Gözüaçık and Can (2021)), and Half-Space Trees (Wetzig et al. (2019); Lyu et al. (2020)).

The main contribution of the proposed solution to the developed body of research is that it:

- Enriches interpretable anomaly detection with adaptive capabilities
- Isolates root cause of anomalies while considering interactions
- Uses self-learning approach on streamed IoT data
- Demonstrates interpretability by providing process limits for signals
- Blends with existing SCADA architecture

### 1.5. Paper Organization

The rest of the paper is structured as follows: We begin with the problem and motivation in **Section 1**, providing context. Next, in **Section 2**, we lay the theoretical groundwork. Our proposed adaptive anomaly detection method is detailed in **Section 3**. We then demonstrate real-world industrial-scale applications in **Section 4**. Finally, we conclude the paper in **Section 5**, summarizing findings and discussing future research directions.

## 2. Preliminaries

In this section, we present the fundamental ideas that form the basis of the developed approach. Subsection 2.1 explains Welford’s online algorithm, which can adjust distribution to changes in real-time. Subsection 2.2 proposes a two-pass implementation that can reverse the impact of expired samples. The math behind distribution modeling in Subsection 2.3 establishes the foundation for the Gaussian anomaly detection model discussed in Subsection 2.5, followed by conditional probability computation in Subsection 2.4. The last subsection of the preliminaries is devoted to the definition of anomalies.

214    2.1. Welford's Online Algorithm

215    Welford introduced a numerically stable online algorithm for calculating  
 216    mean and variance in a single pass through data. Therefore, the algorithm  
 217    allows the processing of IoT device measurements without the need to store  
 218    their values Welford (1962).

219    Given measurement  $x_i$  where  $i = 1, \dots, n$  is a sample index in sample  
 220    population  $n$ , the corrected sum of squares  $S_n$  is defined as

$$S_n = \sum_{i=1}^n (x_i - \bar{x}_n)^2, \quad (1)$$

221    with the running mean  $\bar{x}_n$  defined as previous mean  $\bar{x}_{n-1}$  weighted by pro-  
 222    portion of previously seen population  $n - 1$  corrected by current sample as

$$\bar{x}_n = \frac{n-1}{n} \bar{x}_{n-1} + \frac{1}{n} x_n = \bar{x}_{n-1} + \frac{x_n - \bar{x}_{n-1}}{n}. \quad (2)$$

223    Throughout this paper, we consider the following formulation of an update  
 224    to the corrected sum of squares:

$$S_n = S_{n-1} + (x_n - \bar{x}_{n-1})(x_n - \bar{x}_n), \quad (3)$$

225    as it is less prone to numerical instability due to catastrophic cancellation,  
 226    significant loss of precision due to subtracting two nearly equal numbers.

227    Finally, the corresponding unbiased variance is

$$s_n^2 = \frac{S_n}{n-1}. \quad (4)$$

228    This implementation of the Welford method requires the storage of three  
 229    scalars:  $\bar{x}_{n-1}$ ;  $n$ ;  $S_n$ .

230    2.2. Inverting Welford's Algorithm

231    Based on (2), it is clear that the influence of the latest sample over the  
 232    running mean decreases as the population  $n$  grows. For this reason, regulat-  
 233    ing the number of samples used for sample mean and variance computa-  
 234    tion has crucial importance over adaptation. Given access to the instances used  
 235    for computation and expiration period  $t_e \in \mathbb{N}_0^{n-1}$ , reverting the impact of  
 236     $x_{n-t_e}$  can be written as follows

$$S_{n-1} = S_n - (x_{n-t_e} - \bar{x}_{n-1})(x_{n-t_e} - \bar{x}_n), \quad (5)$$

237 where the reverted mean is given as

$$\bar{x}_{n-1} = \frac{n}{n-1}\bar{x}_n - \frac{1}{n-1}x_{n-t_e} = \bar{x}_n - \frac{x_{n-t_e} - \bar{x}_n}{n-1}. \quad (6)$$

238 Finally, the unbiased variance follows the formula:

$$s_{n-1}^2 = \frac{S_{n-1}}{n-2}. \quad (7)$$

239 Notably, inversion allows the algorithm to keep a constant rate of adap-  
240 tation at the cost of storing a bounded data buffer.

### 241 2.3. Statistical Model of Multivariate System

242 Multivariate normal distribution generalizes the multivariate systems to  
243 the model where the degree to which variables are related is represented by  
244 the covariance matrix. Gaussian normal distribution of variables is a reason-  
245 able assumption for process measurements, as it is a common distribution  
246 that arises from stable physical processes measured with noise (Mishra and  
247 Datta-Gupta (2018)). The general notation of multivariate normal distribu-  
248 tion is:

$$\mathbf{X} \sim \mathcal{N}_k(\boldsymbol{\mu}, \boldsymbol{\Sigma}), \quad (8)$$

249 where  $k$ -dimensional mean vector is denoted as  $\boldsymbol{\mu} = (\bar{x}_1, \dots, \bar{x}_k)^T \in \mathbb{R}^k$   
250 and  $\boldsymbol{\Sigma} \in \mathbb{R}^{k \times k}$  is the  $k \times k$  covariance matrix, where  $k$  is the index of last  
251 random variable.

252 The probability density function (PDF)  $f(\mathbf{x}; \boldsymbol{\mu}, \boldsymbol{\Sigma})$  of multivariate normal  
253 distribution is denoted as:

$$f(\mathbf{x}; \boldsymbol{\mu}, \boldsymbol{\Sigma}) = \frac{1}{(2\pi)^{k/2} |\boldsymbol{\Sigma}|^{1/2}} e^{-\frac{1}{2}(\mathbf{x}-\boldsymbol{\mu})^\top \boldsymbol{\Sigma}^{-1}(\mathbf{x}-\boldsymbol{\mu})}, \quad (9)$$

254 where  $\mathbf{x}$  is a  $k$ -dimensional vector of measurements  $x_i$  at time  $i$ ,  $|\boldsymbol{\Sigma}|$   
255 denotes the determinant of  $\boldsymbol{\Sigma}$ , and  $\boldsymbol{\Sigma}^{-1}$  is the inverse of  $\boldsymbol{\Sigma}$ .

256 The cumulative distribution function (CDF) of a multivariate Gaussian  
257 distribution describes the probability that all components of the random  
258 vector  $\mathbf{X}$  take on a value less than or equal to a particular point  $q$  in space,  
259 and can be used to evaluate the likelihood of observing a particular set of  
260 measurements or data points. In other words, it gives the probability of

261 observing a random vector that falls within a certain region of space. The  
262 standard notation of CDF is as follows:

$$F(\mathbf{x}; \boldsymbol{\mu}, \boldsymbol{\Sigma}) = \int_{-\infty}^q f(\mathbf{x}; \boldsymbol{\mu}, \boldsymbol{\Sigma}) d\mathbf{x}, \quad (10)$$

263 where  $d\mathbf{x}$  denotes the integration over all  $k$  dimensions of  $\mathbf{x}$ .

264 As the equation (10) cannot be integrated explicitly, an algorithm for  
265 numerical computation was proposed in Genz (2000).

266 Given the PDF, we can also determine the value of  $\mathbf{x}$  that corresponds to a  
267 given quantile  $q$  using a numerical method for inversion of CDF (ICDF) often  
268 denoted as percent point function (PPF) or  $F(\mathbf{x}; \boldsymbol{\mu}, \boldsymbol{\Sigma})^{-1}$ . An algorithm that  
269 calculates the value of the PPF is part of standard statistical software tools.

#### 270 2.4. Conditional Probability Distribution

271 Considering that we observe particular vector  $\mathbf{x}_i$ , we can update probabil-  
272 ity distributions, calculated according to the rules of conditional probability,  
273 of individual measurements within the vector given the rest of the measure-  
274 ments in  $\mathbf{x}_i$ . Let's assume multivariate normal distribution (8) and without  
275 loss of generality, that the vector  $\mathbf{x}_i$  can be partitioned into subset variable  
276  $x_a$ , and complement vector  $\mathbf{x}_b$  as follows

$$\mathbf{x}_i = \begin{bmatrix} x_a \\ \mathbf{x}_b \end{bmatrix} \text{ with dimensions } \begin{bmatrix} 1 \times 1 \\ (k-1) \times 1 \end{bmatrix}, \quad (11)$$

277 where  $a = 1, \dots, k$  and  $\mathbf{b} = \{1, 2, \dots, k\}$  where  $a \notin \mathbf{b}$ . This partitioning  
278 allows us to define block-wise mean and covariance as follows:

$$\boldsymbol{\mu} = \begin{bmatrix} \mu_a \\ \boldsymbol{\mu}_b \end{bmatrix} \text{ with dimensions } \begin{bmatrix} 1 \times 1 \\ (k-1) \times 1 \end{bmatrix}, \quad (12)$$

279 and

$$\boldsymbol{\Sigma} = \begin{bmatrix} \sigma_{aa}^2 & \boldsymbol{\Sigma}_{ab} \\ \boldsymbol{\Sigma}_{ba} & \boldsymbol{\Sigma}_{bb} \end{bmatrix} \text{ with dimensions } \begin{bmatrix} 1 \times 1 & 1 \times (k-1) \\ (k-1) \times 1 & (k-1) \times (k-1) \end{bmatrix}. \quad (13)$$

280 Subsequently, we can derive the conditional distribution of any subset  
281 variable  $x_a$ , given the complementary vector  $\mathbf{x}_b$ . This conditional distribution  
282 conforms to a univariate normal distribution, characterized by:

$$X_a | \mathbf{X}_b \sim \mathcal{N}(\mu_{a|\mathbf{b}}, \sigma_{a|\mathbf{b}}^2). \quad (14)$$

283 where  $\mu_{a|b}$  denotes the conditional mean and  $\sigma_{a|b}^2$  represents the conditional variance. These crucial parameters can be computed by applying the  
 284 Schur complement as follows:  
 285

$$\sigma_{a|b}^2 = \sigma_{aa}^2 - \Sigma_{ab}\Sigma_{bb}^{-1}\Sigma_{ba}, \quad (15)$$

286 for the conditional variance  $\sigma_{a|b}^2$ , while the conditional mean, denoted as  
 287  $\mu_{a|b}$ , is determined by:

$$\mu_{a|b} = \mu_a + \Sigma_{ab}\Sigma_{bb}^{-1}(\mathbf{x}_b - \boldsymbol{\mu}_b). \quad (16)$$

288 The conditional variance  $\sigma_{a|b}^2$  essentially represents the Schur complement  
 289 of  $\Sigma_{bb}$  within the overall covariance matrix  $\Sigma$ .

### 290 2.5. Gaussian Anomaly Detection

291 From a viewpoint of statistics, outliers are commonly denoted as values  
 292 that significantly deviate from the mean. Under the assumption that the  
 293 spatial and temporal characteristics of a system, observed over a moving  
 294 window, can be suitably represented as normally distributed features, we  
 295 assert that any anomaly can be identified as an outlier.

296 In empirical fields like machine learning, the three-sigma rule ( $3\sigma$ ) provides  
 297 a framework for characterizing the region of a distribution within which  
 298 normal values are expected to fall with high confidence. This rule renders  
 299 approximately 0.265% of values in the distribution as anomalous.

300 The  $3\sigma$  rule establishes the probability that any sample  $x_a$  of a random  
 301 vector  $X$  falls within a given CDF over a semi-closed interval as the distance  
 302 from the conditional mean  $\mu_{a|b}$  of 3 conditional variances  $\sigma_{a|b}^2$  and gives an  
 303 approximate value of  $q$  as

$$q = P\{|x_a - \mu_{a|b}| < 3\sigma_{a|b}^2\} = 0.99735. \quad (17)$$

304 Utilizing a probabilistic model of normal behavior, we can determine  
 305 threshold values  $x_l$  and  $x_u$  corresponding to the closed interval of the CDF  
 306 where this probability is established. The inversion of Equation (10) facilitates  
 307 this calculation, yielding:

$$x_l = F((1 - P\{|x_a - \mu_{a|b}| < 3\sigma_{a|b}^2\}); \mu_{a|b}, \sigma_{a|b}^2)^{-1}, \quad (18)$$

308 for the lower limit, and

$$x_u = F((P\{|x_a - \mu_{a|\mathbf{b}}| < 3\sigma_{a|\mathbf{b}}^2\}); \mu_{a|\mathbf{b}}, \sigma_{a|\mathbf{b}}^2)^{-1}, \quad (19)$$

309 for the upper limit. These lower and upper limits together form vectors  
 310  $\mathbf{x}_l$  and  $\mathbf{x}_u$ , respectively, defining the region of normal system operation. This  
 311 region is conceptualized as a hypercube in the feature space, with each di-  
 312 mension bounded by the corresponding feature limits, as computed using  
 313 Equations (18) and (19) for all  $a = 1, \dots, k$ ;  $\mathbf{b} = \{1, 2, \dots, k\}$  where  $a \notin \mathbf{b}$ .  
 314 The approximation of a confidence ellipse as a hypercube can be employed  
 315 to represent the region of normal system operation for individual variables  
 316 of a multivariate system, rendering it as an aid for visual representation.

317 The predicted state of the system, denoted as  $y_i$ , and the normality of  
 318 signals  $\mathbf{y}_{s,i}$  at time  $i$  are determined based on the maximum distance of  
 319 observations from the center of the probabilistic density. The center of the  
 320 probabilistic density corresponds to the vector of conditional means  $\mu_{a|\mathbf{b}}$  with  
 321 respect to other features. The calculation of this distance involves the cumu-  
 322 lative distribution function (CDF) of observations and conditional distribu-  
 323 tions, as follows:

$$F(x_a; \mu_{a|\mathbf{b}}, \sigma_{a|\mathbf{b}}^2) : a = 1, \dots, k; \mathbf{b} = \{1, 2, \dots, k\} \text{ where } a \notin \mathbf{b}. \quad (20)$$

324 Subsequently, operation states of individual inputs are defined as follows:

$$\mathbf{y}_{s,i} = \begin{cases} 0 & \text{if } T \leq (20) \\ 1 & \text{if } T > (20), \end{cases} \quad (21)$$

325 where  $T$  represents a threshold that distinguishes between normal signal  
 326 measurement ( $\mathbf{y}_{s,i} = 0$ ) and abnormal ( $\mathbf{y}_{s,i} = 1$ ).

327 For the overall abnormality of the system, any anomaly in signals  $\mathbf{y}_{s,i}$  is  
 328 considered, resulting in:

$$y_i = \begin{cases} 1 & \text{if } 1 \in \mathbf{y}_{s,i} \\ 0 & \text{otherwise,} \end{cases} \quad (22)$$

329 defining the discrimination boundary between system operation where  
 330  $y_i = 0$  indicates normal system operation, and  $y_i = 1$  indicates anomalous  
 331 operation.

332    *2.6. Anomaly Definition*

333    This subsection provides an overview of the definition of anomalies in  
334    data analysis and their categorization, setting conventions for this paper.

335    In the realm of data analysis, anomalies are conspicuous deviations from  
336    the anticipated patterns within a dataset. Traditionally, the task of anomaly  
337    detection has relied upon unsupervised methodologies, wherein the identifi-  
338    cation of "outliers" entails the comparison of data points in both temporal  
339    and spatial contexts. This approach, often referred to as point-wise anomaly  
340    detection, classifies a data point as an anomaly when it exhibits significant  
341    dissimilarity from its neighboring data points (Iglesias Vázquez et al. (2023)).

342    The concept of point anomalies, influenced by factors such as temporal  
343    and spatial aspects, can be further categorized into conditional and contex-  
344    tual anomalies (Ruff et al. (2021)).

345    Nevertheless, this conventional method may not be suitable for scenarios  
346    characterized by collective anomalies, where clusters of abnormal data points  
347    coexist. A more pragmatic approach defines anomalies as deviations from  
348    established "normal" patterns, resembling the principles of semi-supervised  
349    learning. Change point detection, in a similar vein, can be regarded as a  
350    relative approach that takes into account the varying dynamics of changes,  
351    whether they occur gradually or abruptly (Iglesias Vázquez et al. (2023)).

352    It is imperative to recognize that the interpretation of anomalies, outliers,  
353    and novelties can vary upon the application. Anomalies typically garner  
354    significant attention, while outliers are often treated as undesirable noise  
355    and are typically excluded during data preprocessing. Novelties, on the other  
356    hand, signify new observations that necessitate model updates to adapt to  
357    an evolving environment (Ruff et al. (2021)).

358    Notwithstanding the differences in terminology, methods employed for the  
359    identification of data points residing in low-probability regions, irrespective  
360    of whether they are referred to as "anomaly detection," "outlier detection,"  
361    or "novelty detection," share fundamental similarities (Iglesias Vázquez et al.  
362    (2023)).

363    **3. Adaptive Anomaly Detection and Interpretation Framework**

364    In this section, we propose an adaptive and interpretable detection frame-  
365    work (AID) for multivariate systems with streaming IoT devices. This ap-  
366    proach models the system as a dynamic joint normal distribution, enabling  
367    it to effectively adapt to pervasive nonstationary effects on processes. Our

368 method handles various factors, including change points, concept drift, and  
369 seasonal effects. Our primary contribution lies in the fusion of an adaptable  
370 self-supervised system with root cause identification capabilities. This combi-  
371 nation empowers the online statistical model to diagnose anomalies through  
372 two distinct mechanisms. Firstly, it employs conditional probability calcu-  
373 lations to assess the system’s operating conditions’ normality. Secondly, it  
374 identifies outliers within individual signal measurements and features based  
375 on dynamic alert-triggering process limits. In the following sections, we de-  
376 scribe our proposed methodology across three subsections. The initial sub-  
377 section delves into the process of initializing the model’s parameters. The  
378 subsequent section describes online training and adaptation, while the final  
379 subsection expounds upon the model’s detection and diagnostic capabilities.  
380 For a concise representation of the proposed method, Algorithm 1 is provided.

381 *3.1. Model Parameters Initialization*

382 The model initialization is governed by defining two tunable hyperparam-  
383 eters of the model: the expiration period ( $t_e$ ) and the threshold ( $T$ ). The  
384 expiration period determines the window size for time-rolling computations,  
385 impacting the proportion of outliers within a given timeframe, and directly  
386 influencing the relaxation (with a longer expiration period) or tightening  
387 (with a shorter expiration period) of dynamic signal limits. Additionally, we  
388 introduce a grace period, which defaults to  $3/4t_e$ , allowing for model calibra-  
389 tion. During this grace period, system anomalies are not flagged to prevent  
390 false positives and speed up self-supervised learning, introduced in Subsec-  
391 tion 3.2. The length of the expiration period inversely correlates with the  
392 model’s ability to adapt to sudden changes. The adaptation and detection  
393 of shifts in the data-generating process, such as changes in mean or variance,  
394 is managed through the adaptation period  $t_a$ . A longer  $t_a$  results in slower  
395 adaptation but potentially longer alerts, which can be valuable when collec-  
396 tive anomalies are expected to occur. In most cases,  $t_a = t_e$  offers optimal  
397 performance.

398 As a general rule of thumb, expiration period  $t_e$  should be determined  
399 based on the slowest observed dynamics within the multivariate system. The  
400 threshold  $T$  defaults to the three-sigma probability of  $q$  in (17). Adjusting  
401 this threshold can fine-tune the trade-off between precision and recall. A  
402 lower threshold boosts recall but may lower precision, while a higher thresh-  
403 old enhances precision at the cost of recall. The presence of one non-default

404 easily interpretable hyperparameter facilitates adaptability to various sce-  
405 narios. We recommend starting with the default values of other parameters  
406 and making adjustments based on real-time model performance.

407 *3.2. Online training*

408 AID training follows an incremental learning approach, processing each  
409 new sample upon arrival. Incremental learning allows online parameter up-  
410 dates, albeit with a potential computational delay affecting response latency.

411 In the case of a dynamic joint probability distribution, the parameters are  
412  $\mu_i$  and  $\Sigma_i$  at time instance  $i$ . Update of the mean vector  $\mu_i$  and covariance  
413 matrix  $\Sigma_i$  is governed by Welford's online algorithm using equation (2) and  
414 (4) respectively. Samples beyond the expiration period  $t_e$  are disregarded  
415 during the second pass. The effect of expired samples is reverted using inverse  
416 Welford's algorithm for mean (6) and variance (7), accessing the data in the  
417 buffer. For details, refer to Subsection 2.2.

418 It is worth noting that adaptation relies on two self-supervised methods.  
419 Adaptation routine runs if the observation at time instance  $i$  is considered  
420 normal. Furthermore, adaptation period  $t_a$  allows the model to update the  
421 distribution on collective anomalies as well, thus speeding up the adaptation  
422 to change points. Given the predicted system anomaly state from (22) as  $y_i$   
423 over the window of past observations  $\mathbf{y}_i = \{y_{i-t_a}, \dots, y_i\}$ , the following test  
424 holds when adaptation is performed on outlier:

$$\frac{\sum_{y \in \mathbf{y}_i} y}{n(\mathbf{y}_i)} > T. \quad (23)$$

425 Here  $n(\mathbf{y}_i)$  denotes the dimensionality of  $\mathbf{y}_i$ . The logic of the (23) follows  
426 that over an adaptation period  $t_a$ , the changepoint can be discriminated from  
427 collective anomalies and point anomalies by their minimum duration, while  
428  $T$  allows some overlap with previous normal conditions.

429 *3.3. Online prediction*

430 In the prediction phase, multiple metrics are evaluated to assess the state  
431 of the modeled system.

432 Firstly, we calculate the parameters of the conditional distribution con-  
433 cerning the dynamic multivariate Gaussian distribution. These calculations

434 are performed for the process observation vector  $\mathbf{x}_i$  at time instance  $i$ . Specifically,  
435 we compute the conditional mean using (16) and the conditional variance  
436 using (15). These computations yield univariate conditional distributions  
437 for individual signals and features. These conditional distributions play  
438 a crucial role in assessing the abnormality of signals and features concerning  
439 other observed values. This assessment relies on the strength of relationships  
440 defined by the covariance matrix of the dynamic multivariate Gaussian  
441 distribution. Consequently, our approach inherently considers the interactions  
442 between input signals and features. The determination of anomalous  
443 behavior is governed by (21).

444 Any anomaly detected within one of the features triggers an alert at the  
445 system level. The decision regarding the overall system's anomalous behavior  
446 is guided by (22). Nevertheless, individual determinations of anomalies serve  
447 as a diagnostic tool for isolating the root cause of anomalies.

448 To assist operators in their assessments, we establish a hypercube defined  
449 by lower and upper threshold values, denoted as  $\mathbf{x}_l$  and  $\mathbf{x}_u$ , respectively.  
450 These thresholds are derived from (18) and (19), incorporating updated  
451 model parameters. Lower and upper thresholds play a pivotal role as dynamic  
452 process limits. They replace the conservative process limits provided  
453 in sensor documentation, accounting for spatial factors, such as multipoint  
454 measurements, temporal factors such as aging, and actual environmental  
455 conditions that influence sensor operation.

456 Our framework anticipates unexpected novel behavior, including signal  
457 loss. This anticipation involves calculating the cumulative distribution function  
458 (CDF) over the univariate normal distribution of sampling, focusing  
459 on the differences between subsequent timestamps. We operate under the  
460 assumption that, over the long term, the distribution of sampling times remains  
461 stable. As a result, we employ a one-pass update mechanism utilizing  
462 (2) and (4), for efficiency. To proactively detect subtle changes in sampling  
463 patterns, self-supervised learning is employed, leveraging anomalies weighted  
464 by the deviation from  $(1 - F(x_i; \mu, \sigma^2))$  for training.

465 The system is vigilant in identifying change points. When the adaptation  
466 test specified in (23) is satisfied, change points are flagged and isolated.  
467 This initiation of change points triggers updates to the model, as stated in  
468 Subsection 3.2. ensuring it adapts to evolving data patterns, such as changes  
469 in operation state, effectively.

---

**Algorithm 1** Online Detection and Identification Workflow

---

**Input:** expiration period  $t_e$

**Output:** system anomaly  $y_i$ , signal anomalies  $\mathbf{y}_{s,i}$ , sampling anomaly  $y_{t,i}$ , change-point  $y_{c,i}$ , lower thresholds  $\mathbf{x}_{l,i}$ , upper thresholds  $\mathbf{x}_{u,i}$ ,

*Initialisation :*

- 1:  $i \leftarrow 1; n \leftarrow 1; T \leftarrow (17); \boldsymbol{\mu} \leftarrow \mathbf{x}_0; \boldsymbol{\Sigma} \leftarrow \mathbf{1}_{k \times k}; \mu_t \leftarrow 0; \sigma_t^2 \leftarrow 1;$
  - 2: compute  $F(\mathbf{x}_0; \boldsymbol{\mu}, \boldsymbol{\Sigma})$  using algorithm in Genz (2000);  
*LOOP Process*
  - 3: **loop**
  - 4:    $\mathbf{x}_i, t_i \leftarrow \text{RECEIVE}();$
  - 5:    $\mathbf{y}_{s,i} \leftarrow \text{PREDICT}(\mathbf{x}_i, T)$  using (21);
  - 6:    $y_i \leftarrow \text{PREDICT}(\mathbf{y}_{s,i})$  using (22);
  - 7:    $\mathbf{x}_{l,i}, \mathbf{x}_{u,i} \leftarrow \text{GET}(T, \boldsymbol{\mu}, \boldsymbol{\Sigma})$  using (18), (19);
  - 8:    $y_{t,i} \leftarrow \text{PREDICT}(t_i - t_{i-1})$  using (21);
  - 9:    $\mu_t, \sigma_t^2 \leftarrow \text{UPDATE}(t_i - t_{i-1}, \mu_t, \sigma_t^2)$  using (2), (4);
  - 10:   **if** (22) = 0 **or** (23) **then**
  - 11:      $\boldsymbol{\mu}, \boldsymbol{\Sigma} \leftarrow \text{UPDATE}(\mathbf{x}_i, \boldsymbol{\mu}, \boldsymbol{\Sigma}, n)$  using (2), (4);
  - 12:     **if** (23) **then**
  - 13:        $y_{c,i} \leftarrow 1;$
  - 14:     **else**
  - 15:        $y_{c,i} \leftarrow 0;$
  - 16:     **end if**
  - 17:      $n \leftarrow n + 1;$
  - 18:     **for**  $\mathbf{x}_{i-t_e}$  **do**
  - 19:        $\boldsymbol{\mu}, \boldsymbol{\Sigma} \leftarrow \text{REVERT}(\mathbf{x}_{i-t_e}, \boldsymbol{\mu}, \boldsymbol{\Sigma}, n)$  using (6), (7);
  - 20:        $n \leftarrow n - 1;$
  - 21:     **end for**
  - 22:   **end if**
  - 23:    $i \leftarrow i + 1;$
  - 24: **end loop**
- 

<sup>470</sup> **4. Case Study**

<sup>471</sup> This section presents two case studies on real industrial-scale energy stor-  
<sup>472</sup> ages and a real data benchmark to demonstrate the effectiveness and appli-  
<sup>473</sup>ability of our proposed approach. We investigate the properties and per-  
<sup>474</sup>formance of the approach using signals from IoT devices in an energy system

475 and streamed benchmark system data. The successful deployment demon-  
476 strates that this approach is suitable for existing industrial systems utilizing  
477 IoT data streams on top of well-established SCADA systems.

478 *4.1. Battery Energy Storage System TERRA*

479 In the first case study, we demonstrate our proposed method on real  
480 industrial-scale battery energy storage system (BESS) TERRA, depicted in  
481 Fig 1. TERRA has an installed capacity of 151 kWh distributed among  
482 10 modules with 20 cells. The Inverter's nominal power is 100 kW. The  
483 TERRA reports measurements of State of Charge (SoC), supply/draw energy  
484 set-points, and inner temperature, at 6 positions (channels) of each battery  
485 module. A substantial size of the system, which is 2.4x2.4x1.2m (HxWxD),  
486 requires a proper cooling mechanism. The cooling is handled by forced air  
487 from the HVAC system and inner fans, while the fire safety system is passive.  
488 Tight battery temperature control is needed to optimize performance and  
489 maximize the safety and battery's lifespan. Identifying anomalous events  
490 and removal of corrupted data might yield significant improvement in the  
491 process control level and increase the reliability and stability of the system.



Figure 1: Photograph of the actual studied TERRA energy storage unit with open doors (left), and closed doors (right).

492 The AID is integrated into the existing software infrastructure of the  
493 system, allowing detection and diagnosis of the system using streamed IoT

494 data. Here we replay a 9-day stream of historical measurements of the device,  
495 to demonstrate key features of AID.

496 For demonstration purposes, the expiration period  $t_e$  is set to 4 days, as  
497 the system is expected to adapt to the new behavior, due to the transfer of  
498 the module to the outside. The grace period was reduced to 1 day, to observe  
499 the reaction to concept drift. The threshold  $T$  is set to  $3.5\sigma$  to reduce the  
500 number of alarms. The frequency will be higher as the detector is protected  
501 and self-supervised. The adaptation period  $t_a$  is changed to 3 hours as this  
502 is the time constant of the temperature to the unit change of supply/draw  
503 power demand.

504 Figure 2 depicts the average cell temperature measurement of the TERRA  
505 for all 10 modules. The data are normalized to the range [0, 1] to protect  
506 the sensitive business value. The light red area represents the region out of  
507 dynamic operating limits as provided by AID. On 7<sup>th</sup> March 2022, the system  
508 was relocated from the inside of the building to the outside power socket. The  
509 system was expected to adapt to the new behavior within 4 days as specified  
510 by  $t_e$ . Nevertheless, due to the protection of the model from learning the  
511 anomalous data, the new behavior could not be captured as the system was  
512 not operating within the safe limits. The adaptation started three days later,  
513 as only some of the measurements within the safe region after transfer were  
514 learned. Therefore, the importance of self-supervised adaptation to changes  
515 in data is crucial. As we can see, the change points detection according to  
516 (23) alerted such change shortly after the TERRA was connected to a data  
517 broker, while the length of the adaptation period enabled discrimination from  
518 collective anomaly.

519 In Figure 3 we depict the same measurement with a changepoint adap-  
520 tation mechanism in place. The mechanism speeds up the adaptation to the  
521 new behavior, as the system is allowed to learn from anomalous data when  
522 they represent the changed behavior. The adaptation took approximately 6  
523 times shorter.

524 The default sampling rate of the incoming signal measurements is 1  
525 minute. However, network communication of the IoT devices is prone to  
526 packet dropout, which results in unexpected non-uniformities in sampling  
527 from the perspective of the SCADA system. The transfer of TERRA was  
528 accompanied by the disconnection of IoT sensors from the data broker which  
529 might be considered an anomaly. The system can detect such anomalies as  
530 well, as depicted in Figure 4. Along with known disconnection, the system  
531 alerted two more non-uniformities of shorter extend, scaled in the figure for

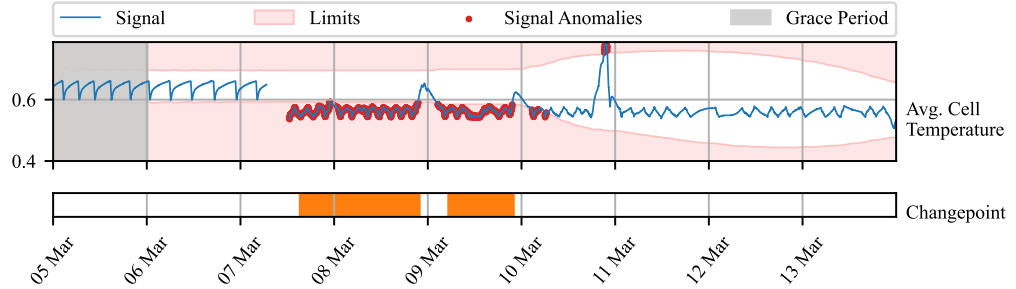


Figure 2: Time series of TERRA measurements observed over 9 days (blue line). The y-axis renders the average temperature of all cells and modules after the normalization to the range of [0, 1]. The light red area represents an area out of dynamic operating limits for individual signals. Observations out of the limits are marked by a red dot. Orange bars represent the times, at which changepoints were detected. Grace period is grayed out.

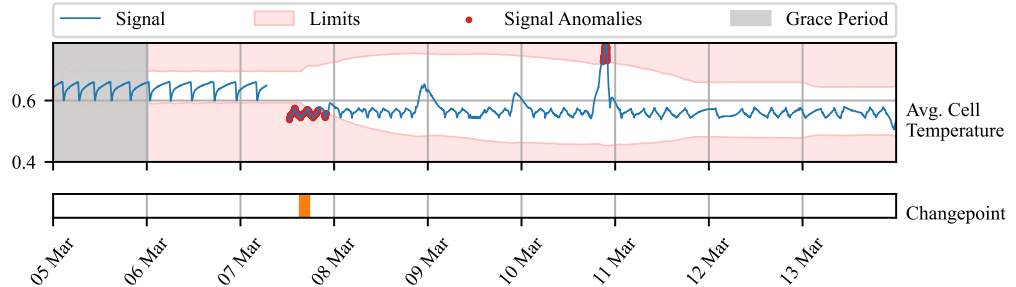


Figure 3: Time series of TERRA measurements observed over 9 days (blue line). The y-axis renders the average temperature of all cells and modules after the normalization to the range of [0, 1]. The light red area represents an area out of dynamic operating limits for individual signals. Observations out of the limits are marked by a red dot. Orange bars represent the times, at which changepoints were detected. Grace period is grayed out.

532 better visibility. The short loss of signal was caused by the packet drop, as  
 533 it impacted only a few consecutive measurements. Various confidence levels  
 534 could be used to further analyze and map potential causes to the duration  
 535 of the outage.

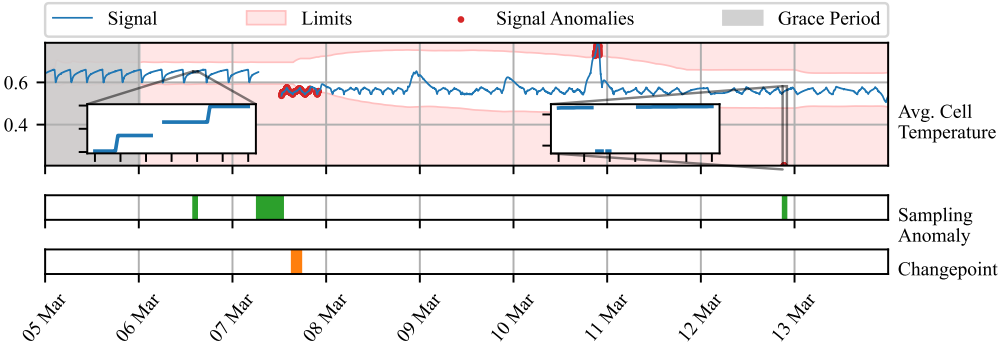


Figure 4: Time series of TERRA measurements observed over 9 days (blue line). The y-axis renders the average temperature of all cells and modules after the normalization to the range of [0, 1]. The light red area represents an area out of dynamic operating limits for individual signals. Observations out of the limits are marked by a red dot. Orange bars represent the times, at which changepoints were detected. Green bars represent periods where sampling anomaly was alerted. Grace period is grayed out.

536 Lastly, we want to acknowledge the outlier, left uncaptured due to in-  
 537 creased variance of the distribution in a period of adaptation. Observing  
 538 multiple variables, where some might be influenced less by the change in be-  
 539 havior, might be beneficial in such cases. The industrial partner provided a  
 540 physical model of the battery module temperature, defined as follows:

$$\begin{aligned} T_{\text{bat},i+1} = & T_{\text{bat},i} + T_s(q_{\text{fan}} V_{\text{b,max}} \rho c_p (T_{\text{out}} - T_{\text{bat},i}) + V_{\text{c,max}} q_{\text{circ.fan}} \rho c_p T_{\text{bat},i} \\ & + q_{\text{circ.fan}} (P_{\text{cool}} q_{\text{cool}} P_{\text{heat}} q_{\text{heat}}) + c_{\text{scale}} Q_{\text{bat}} + q_{\text{inner fans}} \\ & - (V_{\text{b,max}} q_{\text{fan}} V_{\text{c,max}} q_{\text{circ.fan}}) \rho c_p T_{\text{bat},i}) / (m_{\text{bat}} c_{\text{p,b}}) \end{aligned} \quad (24)$$

541 When combined with an averaged measurement of battery module tem-  
 542 perature, we could compute the difference between real and predicted tem-  
 543 perature. Such deviation can be useful in detecting unexpected patterns in  
 544 temperature due to the impact of external disturbance and aging. Neverthe-  
 545 less, it may be inaccurate as the physical model is simplified and does not  
 546 account for spatial aspects, like temperature gradients as well as different

dynamic effects of charging and discharging on temperature. For instance, in Fig. 1 during the first two days we see, that the cooling dynamic is not captured well, resulting in a subtle positive difference between average cell temperature and the temperature predicted by the model. In combination with the raw measured average of the temperature, the AID captures the outlier on 9<sup>th</sup> March which could not be captured in a univariate setting. The physical model exposes temporal aspects of the behavior as it considers the dynamics of its inputs. The rapid increase in temperature w.r.t the modeled dynamics due to environmental conditions will draw a sharp positive peak in the difference between the real and predicted temperature, which will slowly vanish. Based on the significance of the deviation, the peak will be notified as a single-point anomaly or collective anomaly.

This case study demonstrated AID’s effectiveness within the context of the energy storage system, specifically the TERRA system. The AID system exhibited adaptability to changes in the operational environment, contributing to its versatility and robustness. Additionally, it facilitated the establishment of dynamic operating limits for SCADA systems, considering context of the device such as environmental conditions or aging. Furthermore, the AID system showcased its capability to operate with a physical model, enhancing the precision of anomaly detection processes. This highlights the potential of AID as a valuable tool within complex industrial systems.

#### 4.2. Kokam Battery Module

A second case study presents temperature profile monitoring of individual modules of battery pack TERRA deployed at the premises of the end user. During the operation, a hardware fault of module’s 9 cooling fan occurred on 23<sup>rd</sup> August 2023 at 17:12:30. Our industrial partner was interested in finding out, whether such an event could be captured by an anomaly detection system. Each of the 10 modules, embodies 20 cells measured by 6 spatially distributed sensors as shown in Figure 6. The measurements are sent in 30-second intervals and processed in a streamed manner by SCADA. With the availability of the temperature profiles for all the modules, we computed the deviation of the observed value from the average of all the modules’ temperature measurements. The ground truth information about the fan fault was provided to the best of the operator’s knowledge. However, this information serves for evaluation only, as the system operates in a self-supervised manner.

Our anomaly detection system was, in this case, initialized for the operation in production. The expiration period of 7 days, allowed the system

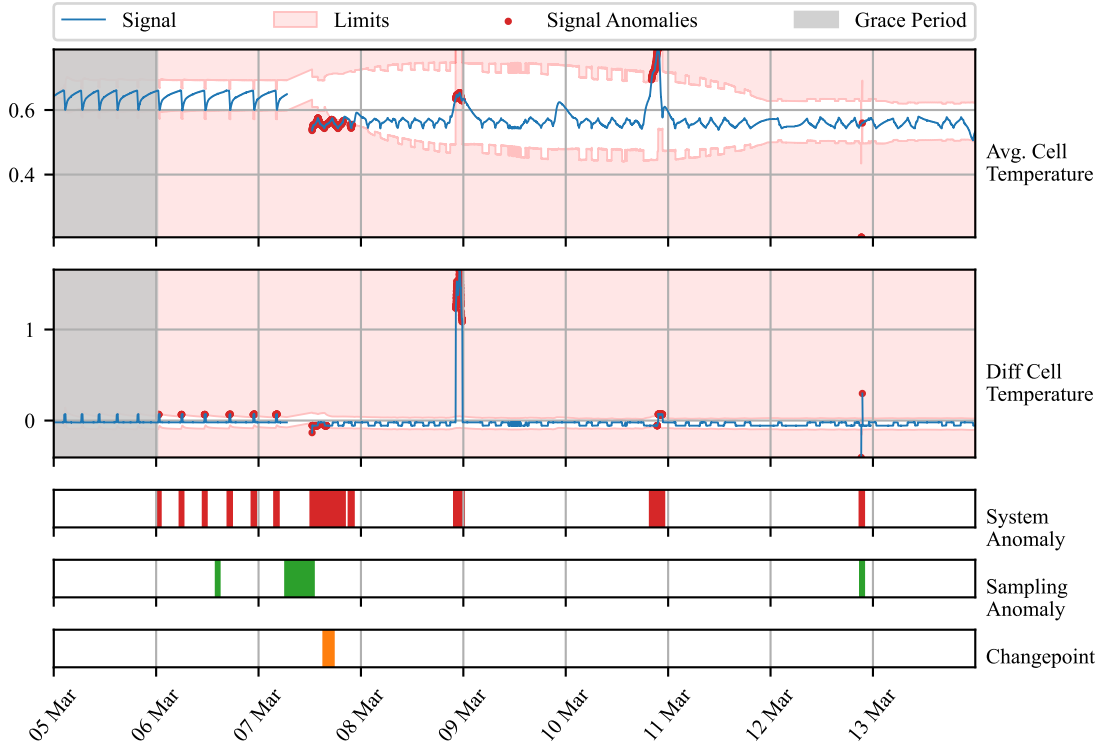


Figure 5: Time series of TERRA measurements observed over 9 days (blue line). The y-axis renders the average temperature of all cells and modules after the normalization to the range of  $[0, 1]$ . The light red area represents an area out of dynamic operating limits for individual signals. Observations out of the limits are marked by a red dot. Orange bars represent the times, at which changepoints were detected. Green bars represent periods where sampling anomaly was alerted. Red bars denote the period where any of the signals contained anomaly. Grace period is grayed out.

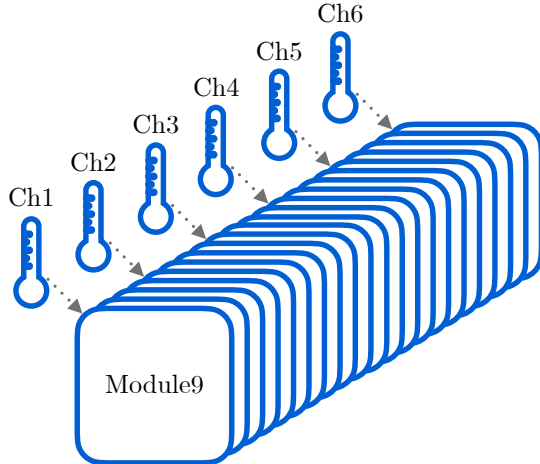


Figure 6: Module 9 with 20 cells and 6 sensors measuring the temperature at each 4<sup>th</sup> cell.

584 to adapt to weekly seasonality due to the usage of the battery following  
 585 work week. The grace period was kept at the default value, equal to  $t_e$ . The  
 586 threshold value was shifted to a 4 sigma value of 99.977% which makes the the  
 587 frequency of anomalous events approximately once a week given 30-second  
 588 sampling. The adaptation period was held constant as the deployed system  
 589 is not expected to change its behavior dramatically on a daily basis.

590 In Figure 7 we observe 4 days of operation around the period of fan  
 591 fault occurrence. The deviations between the observed temperature mea-  
 592 sured by channels of module 9 and the average temperature of all modules  
 593 are displayed. The dynamic operating limits tightly envelop temperatures  
 594 measured by the sensors in the middle of the module (refer to Figure 6),  
 595 while measurements at both sides deviate more due to the proximity to the  
 596 walls and sources of disturbance. We observed multiple alarms raised by var-  
 597 ious channels individually before the fan fault. These anomalies, while not  
 598 addressed here further, could be subjects of interest for further investigation  
 599 by system operators. Meanwhile, the fan fault at the center of our focus is  
 600 alarmed based on three measurements, namely channels 1, 2, and 3. From  
 601 the zoomed views, we can observe a sharp increase in the temperature devia-  
 602 tion. The alarm is on until 24<sup>th</sup> August at noon, when significant fluctuations  
 603 vanish followed by temporary settling of the temperature. On 25<sup>th</sup> August

604 at 11:21, increased temperature fluctuations are followed by an increase of  
605 temperature similar to the initial one. AID alerts this fault again based on  
606 measurements by channels 1, 2, and 3.

607 Time series of TERRA measurements observed over 9 days (blue line).  
608 The y-axis renders the average temperature of all cells and modules after the  
609 normalization to the range of [0, 1]. The light red area represents an area out  
610 of dynamic operating limits for individual signals. Observations out of the  
611 limits are marked by a red dot. Orange bars represent the times, at which  
612 changepoints were detected. Green bars represent periods where sampling  
613 anomaly was alerted. Red bars denote the period where any of the signals  
614 contained anomaly. Grace period is grayed out.

615 Interestingly, during the presence of a fault in the fan, two more peri-  
616 ods where the fan started operating again followed as depicted in Figure 8.  
617 Periods of operation were interrupted again on 27<sup>th</sup> and 28<sup>th</sup> August respec-  
618 tively in the early morning hours. In both of the cases, AID detected the  
619 presence of the fault at the moment of occurrence. In the first case, channel  
620 3 reported an anomaly slightly before the increase in temperature, due to  
621 abnormal fluctuation happening prior to faults.

622 This case study demonstrates the effectiveness of the AID framework in  
623 identifying hardware faults within the context of energy storage systems. It  
624 showcases the system's ability to harness spatially distributed sensors that  
625 measure the same process variable. The AID system successfully pinpointed  
626 a fault in a cooling fan during real-world production operations, underlining  
627 its practical utility and its relevance in enhancing the safety of energy storage  
628 systems. Furthermore, the incorporation of adaptation mechanisms ensures  
629 that the system can be deployed over extended periods without necessitating  
630 resource-intensive retraining. Additionally, the concept of dynamic operating  
631 limits introduced in this study holds promise for integration with Supervisory  
632 Control and Data Acquisition (SCADA) monitoring systems, enabling proac-  
633 tive responses in situations where human life, equipment, or the environment  
634 may be at risk.

#### 635 *4.3. Real Data Benchmark*

636 The benchmarking comparison in this subsection evaluates the AID frame-  
637 work against adaptive unsupervised detection methods, specifically One-  
638 Class Support Vector Machine (OC-SVM) and Half-Space Trees (HS-Trees).  
639 These methods are widely recognized for their iterative learning capabilities

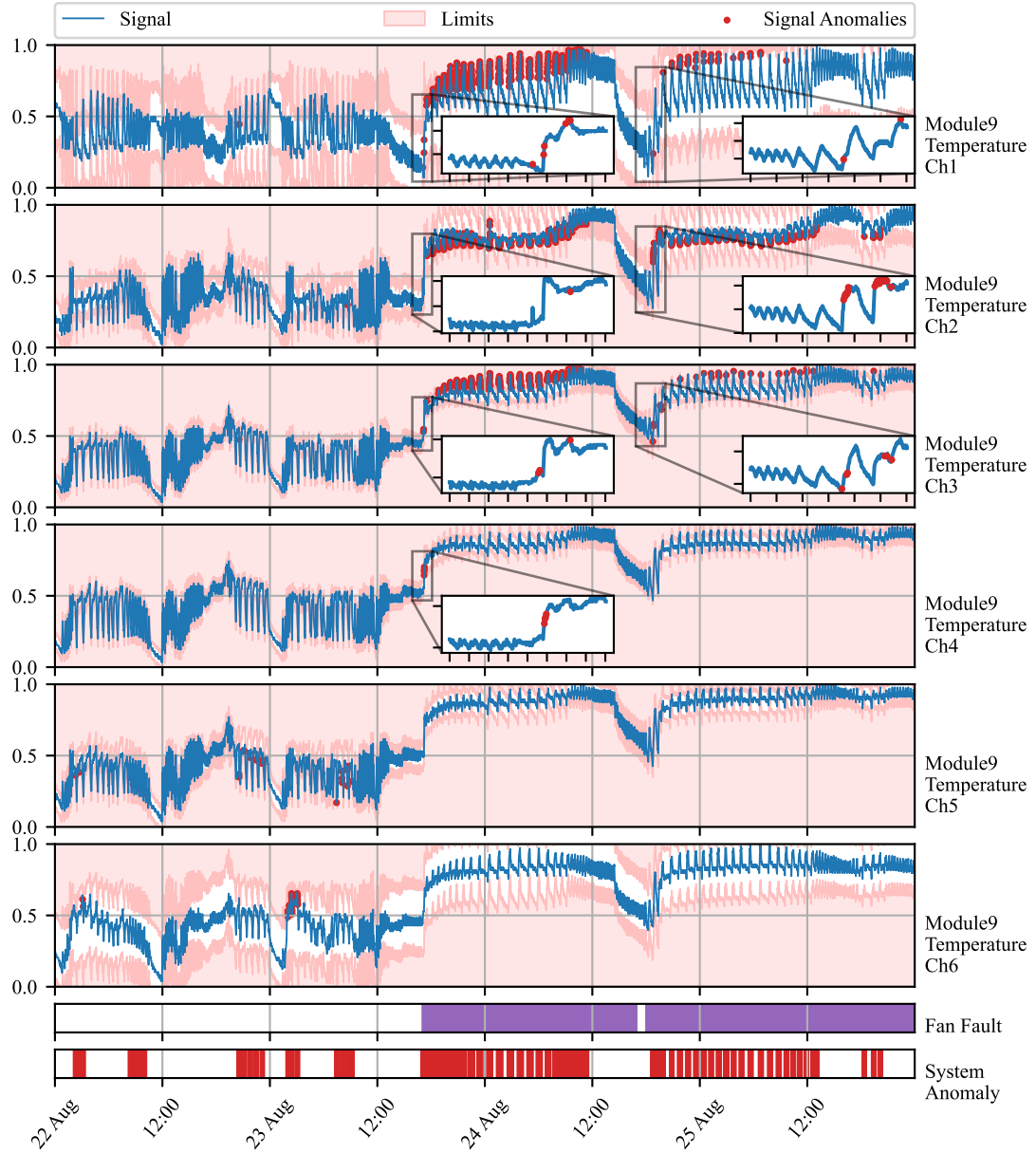


Figure 7: Time series of battery module 9 measurements (blue line). The y-axis renders the normalized deviations of temperature from the average of all modules. Signal anomalies are marked as red dots. The light red area represents an area out of dynamic operating limits. True fan faults are marked by purple bars. Green bars represent the times of changepoint detection. Red bars denote the period where any of the signals contained anomaly.

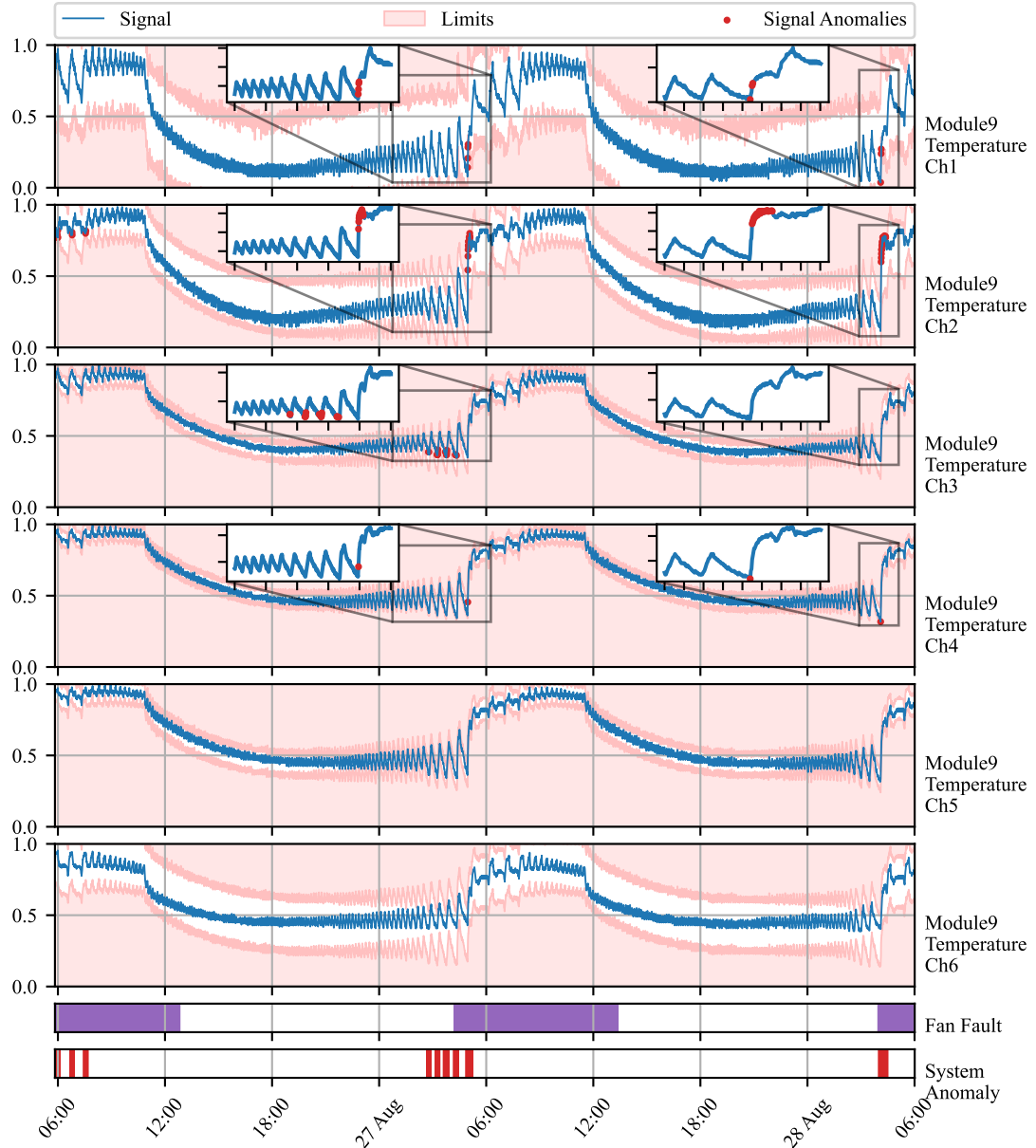


Figure 8: Time series of battery module 9 measurements (blue line). The y-axis renders the normalized deviations of temperature from an average of all modules. Signal anomalies are marked as red dots. The light red area represents an area out of dynamic operating limits. True fan faults are marked by purple bars. Green bars represent the times of changepoint detection. Red bars denote the period where any of the signals contained anomaly.

640 on multivariate time-series data, making them suitable for anomaly detection  
641 in dynamic systems, as previously discussed in the Introduction 1.4.

642 The comparison is based on the Skoltech Anomaly Benchmark (SKAB)  
643 dataset, a real-world dataset with annotated labels distinguishing between  
644 anomalous and normal observations (Katser and Kozitsin (2020)). SKAB  
645 is used for this purpose, as no established benchmarking multivariate data  
646 were found regarding energy storage systems similar to the ones studied in  
647 Subsection 4.1 and Subsection 4.2. The SKAB dataset involves experiments  
648 related to rotor imbalance, where various control actions and changes in  
649 water volume are introduced to the system. It encompasses eight features  
650 and exhibits both gradual and sudden drifts.

651 To ensure fairness in the benchmark, data preprocessing adheres to best  
652 practices for each method. OC-SVM employs standard scaling, while HS-  
653 Trees use normalization. Our proposed AID method requires no scaling.  
654 Preprocessing is performed online, simulating a real production environment,  
655 with running mean and variance for standard scaling and running peak-to-  
656 peak distance for normalization, as supported by the online machine learning  
657 library "river" (Montiel et al. (2021)).

658 The optimal hyperparameters for both reference methods are found us-  
659 ing Bayesian Optimization. Due to no further knowledge about the data  
660 generating process, and equity in benchmark, the hyperparameters of our  
661 proposed method were optimized using Bayesian Optimization as well. 20  
662 steps of random exploration with 100 iterations of Bayesian Optimization  
663 were used, increasing default values set in the Bayesian Optimization library,  
664 to allow thorough exploration and increase the possibility of finding global  
665 optima in each case (Nogueira (2014)). The hyperparameters are optimized  
666 with the F1 score as a cost function first, to maximize both precision and  
667 recall on anomalous samples.

668 As adaptation is required and anticipated within benchmark datasets,  
669 the performance is evaluated iteratively, similarly to the operation after de-  
670 ployment. The metric is updated with each new sample and its final value is  
671 used to drive Bayesian Optimization. The performance is evaluated using the  
672 best-performing model, found by Bayesian Optimization. The performance  
673 of the proposed method is evaluated on the same data as the models are  
674 optimized for.

675 Hyperparameter search ranges are specified, with values centered around  
676 default library values for OC-SVM and HS-Trees. The ranges are inten-  
677 tionally set wide to facilitate comprehensive exploration. The quantile filter

678 threshold used in OC-SVM and HS-Trees aligns with the threshold used in  
 679 AID. These hyperparameter ranges are presented in Table 1.

Table 1: Hyperparameter Ranges for Detection Algorithms

Algorithm	Hyperparameters	Default	Ranges
AID	Threshold	0.99735	(0.85, 0.99994)
	$t_e$	-	(150, 10000)
	$t_a$	$t_e$	(50, 2000)
	Grace Period	$t_e$	(50, 1000)
OC-SVM	Threshold	-	(0.85, 0.99994)
	Learning Rate	0.01	(0.005, 0.02)
HS-Trees	Threshold	-	(0.85, 0.99994)
	N Trees	10	(0, 20)
	Max Height	8	(2, 14)
	Window Size	250	(100, 400)

680 The results for models optimized for the F1 score are summarized in Ta-  
 681 ble 2, which includes precision, recall, F1 score, and average latency. Macro  
 682 values are enclosed in brackets, representing the mean of the metric for both  
 683 anomalies and normal data. A perfect detection achieves 100% in each met-  
 684 ric. According to the Scoreboard for various algorithms on SKAB’s Kaggle  
 685 page, all iterative approaches perform comparably to the batch-trained iso-  
 686 lation forest and autoencoder, validating the optimization process. Notably,  
 687 the proposed AID method outperforms both reference methods in terms of  
 688 F1 score, recall, and precision, despite having a 30-fold higher latency per  
 689 sample. This highlights the scalability as a candidate for further develop-  
 690 ment. Nevertheless, in this case, sampling of the benchmark data still offers  
 691 enough time to deliver predictions with sufficient frequency.

692 Optimal hyperparameters found during Bayesian Optimization are de-  
 693 tailed in Table 3. None of the parameters are at the edge of the provided  
 694 ranges, serving as necessary proof of ranges being broad enough. Never-  
 695 theless, sufficient proof is not possible as multiple parameter ranges are not  
 696 bounded by designed limits.

## 697 5. Conclusion

698 In this paper, we demonstrate the capacity of adaptive conditional prob-  
 699 ability distribution to model the normal operation of dynamic systems em-

Table 2: Evaluation of models optimized for F1 score on SKAB dataset (Katser and Kozitsin (2020)). The best-performing model is highlighted in bold. Values in brackets represent macro values of the metric.

Algorithm	Precision [%]	Recall [%]	F1 [%]	Avg. Latency [ms]
AID	<b>41</b> (59)	<b>80</b> (59)	<b>54</b> (53)	1.45
HS-Trees	36 (51)	74 (51)	48 (44)	<b>0.05</b>
OC-SVM	39 (54)	63 (54)	48 (52)	<b>0.05</b>

Table 3: Optimal hyperparameters of methods optimized for F1 score

Algorithm	Hyperparameters	Found
AID	Threshold	0.96442
	$t_e$	1136
	$t_a$	396
	Grace Period	546
OC-SVM	Threshold	0.86411
	Learning Rate	0.01956
HS-Trees	Threshold	0.99715
	N Trees	1
	Max Height	7
	Window Size	283

ploying streaming IoT data and isolate the root cause of anomalies. AID dynamically adapts to non-stationarity by updating multivariate Gaussian distribution parameters over time. Additionally, self-supervision enhances the model by protecting it from the effects of outliers and increasing the speed of adaptation in response to autonomously detected changes in operation.

Our statistical model isolates the root causes of anomalies as extreme deviations from the conditional means vector, considering spatial and temporal effects encoded in features, as demonstrated in our case studies. This approach establishes the system’s operational state by analyzing the distribution of signal measurements, computing the distance from the mean of conditional probability, and setting dynamic process limits based on multivariate distribution parameters. Additionally, the detector alerts for non-uniform sampling due to packet drops and sensor malfunctions. These adaptable lim-

714 its can be seamlessly integrated into SCADA architecture, enhancing context  
715 awareness and enabling plug-and-play compatibility with existing infrastruc-  
716 ture.

717 The ability to detect and identify anomalies in the system, isolate the  
718 root cause of anomaly to specific signal or feature, and identify signal losses  
719 is shown in two case studies on data from operated industrial-scale energy  
720 storages. These case studies highlight the model’s ability to adapt, diag-  
721 nose the root cause of anomalies, and leverage both physical models and  
722 spatially distributed sensors. Unlike many anomaly detection approaches,  
723 the proposed AID method does not require historical data or ground truth  
724 information about anomalies, alleviating the general limitations of detection  
725 methods employed in the energy industry.

726 The benchmark performed on industrial data indicates that our model  
727 provides comparable results to other self-learning adaptable anomaly detec-  
728 tion methods. This is an important property of our model, as it also allows  
729 for root cause isolation.

730 AID represents a significant advancement in the safety and profitability  
731 of evolving systems that utilize well-established SCADA architecture and  
732 streaming IoT data. By providing dynamic operating limits, AID seamlessly  
733 integrates with existing alarm mechanisms commonly employed in SCADA  
734 systems. To the best of our knowledge, this study appears to be one of the  
735 initial attempts to introduce a self-supervised approach for adaptive anomaly  
736 detection and root cause isolation in SCADA-based systems utilizing IoT  
737 data streams.

738 Future work on this method will include improvements to the change point  
739 detection mechanism, reduction in latency for high-dimensional data, and  
740 minimizing the false positive rate, which is a challenge for general plug-and-  
741 play models. We will also explore the ability to operate with non-parametric  
742 models, in contrast to Gaussian distribution.

743 Our framework is openly accessible on GitHub at the following URL:  
744 [https://github.com/MarekWadinger/online\\_outlier\\_detection](https://github.com/MarekWadinger/online_outlier_detection).

745 **References**

- 746 V. Chandola, A. Banerjee, V. Kumar, Anomaly detection: A survey, ACM  
747 Comput. Surv. 41 (2009). URL: <https://doi.org/10.1145/1541880.1541882>. doi:10.1145/1541880.1541882.

- 749 N. Laptev, S. Amizadeh, I. Flint, Generic and scalable framework for auto-  
750 mated time-series anomaly detection, in: Proceedings of the 21th ACM  
751 SIGKDD International Conference on Knowledge Discovery and Data Min-  
752 ing, KDD '15, Association for Computing Machinery, New York, NY,  
753 USA, 2015, pp. 1939–1947. URL: <https://doi.org/10.1145/2783258.2788611>. doi:10.1145/2783258.2788611.
- 755 A. Kejariwal, Introducing practical and robust anomaly  
756 detection in a time series, 2015. URL: [https://blog.twitter.com/engineering/en\\_us/a/2015/introducing-practical-and-robust-anomaly-detection-in-a-time-series](https://blog.twitter.com/engineering/en_us/a/2015/introducing-practical-and-robust-anomaly-detection-in-a-time-series).
- 759 A. A. Cook, G. Misirlı, Z. Fan, Anomaly detection for iot time-series data:  
760 A survey, IEEE Internet of Things Journal 7 (2020) 6481–6494. doi:10.  
761 1109/JIOT.2019.2958185.
- 762 K. Zhang, J. Chen, C.-G. Lee, S. He, An unsupervised spa-  
763 tiotemporal fusion network augmented with random mask and time-  
764 relative information modulation for anomaly detection of machines  
765 with multiple measuring points, Expert Systems with Applica-  
766 tions 237 (2024) 121506. URL: <https://www.sciencedirect.com/science/article/pii/S0957417423020080>. doi:<https://doi.org/10.1016/j.eswa.2023.121506>.
- 769 J. Huang, D. Cheng, S. Zhang, A novel outlier detecting algo-  
770 rithm based on the outlier turning points, Expert Systems with  
771 Applications 231 (2023) 120799. URL: <https://www.sciencedirect.com/science/article/pii/S0957417423013015>. doi:<https://doi.org/10.1016/j.eswa.2023.120799>.
- 774 C. Fan, Y. Sun, Y. Zhao, M. Song, J. Wang, Deep learning-based fea-  
775 ture engineering methods for improved building energy prediction, Ap-  
776 plied Energy 240 (2019) 35–45. URL: <https://www.sciencedirect.com/science/article/pii/S0306261919303496>. doi:<https://doi.org/10.1016/j.apenergy.2019.02.052>.
- 779 P. D. Talagala, R. J. Hyndman, K. Smith-Miles, Anomaly detection  
780 in high-dimensional data, Journal of Computational and Graphi-  
781 cal Statistics 30 (2021) 360–374. URL: <https://doi.org/10.1080/>

- 782 10618600.2020.1807997. doi:10.1080/10618600.2020.1807997.  
783 arXiv:<https://doi.org/10.1080/10618600.2020.1807997>.
- 784 J. Li, Z. Liu, Attribute-weighted outlier detection for mixed data  
785 based on parallel mutual information, Expert Systems with Appli-  
786 cations 236 (2024) 121304. URL: <https://www.sciencedirect.com/science/article/pii/S0957417423018067>. doi:<https://doi.org/10.1016/j.eswa.2023.121304>.
- 789 X. Du, J. Chen, J. Yu, S. Li, Q. Tan, Generative adversar-  
790 ial nets for unsupervised outlier detection, Expert Systems with  
791 Applications 236 (2024) 121161. URL: <https://www.sciencedirect.com/science/article/pii/S0957417423016639>. doi:<https://doi.org/10.1016/j.eswa.2023.121161>.
- 794 M. Salehi, L. Rashidi, A survey on anomaly detection in evolving data:  
795 [with application to forest fire risk prediction], SIGKDD Explor. Newsl.  
796 20 (2018) 13–23. URL: <https://doi.org/10.1145/3229329.3229332>.  
797 doi:10.1145/3229329.3229332.
- 798 N. Barbosa Roa, L. Travé-Massuyès, V. H. Grisales-Palacio, Dy-  
799 clee: Dynamic clustering for tracking evolving environments, Pat-  
800 tern Recognition 94 (2019) 162–186. URL: <https://www.sciencedirect.com/science/article/pii/S0031320319301992>. doi:<https://doi.org/10.1016/j.patcog.2019.05.024>.
- 803 A. G. Tartakovsky, A. S. Polunchenko, G. Sokolov, Efficient computer net-  
804 work anomaly detection by changepoint detection methods, IEEE Journal  
805 of Selected Topics in Signal Processing 7 (2013) 4–11. doi:10.1109/JSTSP.  
806 2012.2233713.
- 807 H. Wu, J. He, M. Tömösközi, Z. Xiang, F. H. Fitzek, In-network processing  
808 for low-latency industrial anomaly detection in softwarized networks, in:  
809 2021 IEEE Global Communications Conference (GLOBECOM), 2021, pp.  
810 01–07. doi:10.1109/GLOBECOM46510.2021.9685489.
- 811 H. S. Pannu, J. Liu, S. Fu, Aad: Adaptive anomaly detection system for cloud  
812 computing infrastructures, in: 2012 IEEE 31st Symposium on Reliable  
813 Distributed Systems, 2012, pp. 396–397. doi:10.1109/SRDS.2012.3.

- 814 S. Ahmad, A. Lavin, S. Purdy, Z. Agha, Unsupervised real-time anomaly  
815 detection for streaming data, Neurocomputing 262 (2017) 134–  
816 147. URL: <https://www.sciencedirect.com/science/article/pii/S0925231217309864>. doi:<https://doi.org/10.1016/j.neucom.2017.04.070>, online Real-Time Learning Strategies for Data Streams.
- 819 H. H. Bosman, G. Iacca, A. Tejada, H. J. Wörtche, A. Liotta, Ensembles  
820 of incremental learners to detect anomalies in ad hoc sensor networks,  
821 Ad Hoc Networks 35 (2015) 14–36. URL: <https://www.sciencedirect.com/science/article/pii/S1570870515001481>. doi:<https://doi.org/10.1016/j.adhoc.2015.07.013>, special Issue on Big Data Inspired Data  
823 Sensing, Processing and Networking Technologies.
- 825 M. Carletti, C. Masiero, A. Beghi, G. A. Susto, Explainable machine learning  
826 in industry 4.0: Evaluating feature importance in anomaly detection to  
827 enable root cause analysis, in: 2019 IEEE International Conference on  
828 Systems, Man and Cybernetics (SMC), 2019, pp. 21–26. doi:[10.1109/SMC.2019.8913901](https://doi.org/10.1109/SMC.2019.8913901).
- 830 Q. P. Nguyen, K. W. Lim, D. M. Divakaran, K. H. Low, M. C. Chan, Gee: A  
831 gradient-based explainable variational autoencoder for network anomaly  
832 detection, in: 2019 IEEE Conference on Communications and Network  
833 Security (CNS), 2019, pp. 91–99. doi:[10.1109/CNS.2019.8802833](https://doi.org/10.1109/CNS.2019.8802833).
- 834 K. Amarasinghe, K. Kenney, M. Manic, Toward explainable deep neural  
835 network based anomaly detection, in: 2018 11th International Conference  
836 on Human System Interaction (HSI), 2018, pp. 311–317. doi:[10.1109/HSI.2018.8430788](https://doi.org/10.1109/HSI.2018.8430788).
- 838 X. Zhang, J. Shi, X. Huang, F. Xiao, M. Yang, J. Huang,  
839 X. Yin, A. Sohail Usmani, G. Chen, Towards deep probabilistic  
840 graph neural network for natural gas leak detection and localiza-  
841 tion without labeled anomaly data, Expert Systems with Appli-  
842 cations 231 (2023) 120542. URL: <https://www.sciencedirect.com/science/article/pii/S0957417423010448>. doi:<https://doi.org/10.1016/j.eswa.2023.120542>.
- 845 W.-T. Yang, M. S. Reis, V. Borodin, M. Juge, A. Roussy, An interpretable  
846 unsupervised bayesian network model for fault detection and diagno-  
847 sis, Control Engineering Practice 127 (2022) 105304. URL: <https://doi.org/10.1016/j.cengprac.2022.105304>.

- 848        [www.sciencedirect.com/science/article/pii/S0967066122001502](http://www.sciencedirect.com/science/article/pii/S0967066122001502).  
849        doi:<https://doi.org/10.1016/j.conengprac.2022.105304>.
- 850        L. C. Brito, G. A. Susto, J. N. Brito, M. A. V. Duarte, Fault diagnosis  
851        using explainable ai: A transfer learning-based approach for rotating  
852        machinery exploiting augmented synthetic data, Expert Systems with  
853        Applications 232 (2023) 120860. URL: <https://www.sciencedirect.com/science/article/pii/S0957417423013623>. doi:<https://doi.org/10.1016/j.eswa.2023.120860>.
- 856        Z. Wu, X. Yang, X. Wei, P. Yuan, Y. Zhang, J. Bai, A self-supervised  
857        anomaly detection algorithm with interpretability, Expert Systems with  
858        Applications 237 (2024) 121539. URL: <https://www.sciencedirect.com/science/article/pii/S0957417423020419>. doi:<https://doi.org/10.1016/j.eswa.2023.121539>.
- 861        M. Wadinger, M. Kvasnica, Real-time outlier detection with dynamic process  
862        limits, in: 2023 24th International Conference on Process Control (PC),  
863        2023, pp. 138–143. doi:[10.1109/PC58330.2023.10217717](https://doi.org/10.1109/PC58330.2023.10217717).
- 864        K. Yamanishi, J.-i. Takeuchi, A unifying framework for detecting outliers and  
865        change points from non-stationary time series data, in: Proceedings of the  
866        Eighth ACM SIGKDD International Conference on Knowledge Discovery  
867        and Data Mining, KDD '02, Association for Computing Machinery, New  
868        York, NY, USA, 2002, pp. 676–681. URL: <https://doi.org/10.1145/775047.775148>. doi:[10.1145/775047.775148](https://doi.org/10.1145/775047.775148).
- 870        K. Yamanishi, J.-i. Takeuchi, G. Williams, P. Milne, On-line unsu-  
871        pervised outlier detection using finite mixtures with discounting learn-  
872        ing algorithms, Data Mining and Knowledge Discovery 8 (2004) 275–  
873        300. URL: <https://doi.org/10.1023/B:DAMI.0000023676.72185.7c>.  
874        doi:[10.1023/B:DAMI.0000023676.72185.7c](https://doi.org/10.1023/B:DAMI.0000023676.72185.7c).
- 875        B. Steenwinckel, Adaptive anomaly detection and root cause analysis by fus-  
876        ing semantics and machine learning, in: A. Gangemi, A. L. Gentile, A. G.  
877        Nuzzolese, S. Rudolph, M. Maleshkova, H. Paulheim, J. Z. Pan, M. Alam  
878        (Eds.), The Semantic Web: ESWC 2018 Satellite Events, Springer Inter-  
879        national Publishing, Cham, 2018, pp. 272–282.

- 880 B. Steenwinckel, D. De Paepe, S. Vanden Hautte, P. Heyvaert, M. Bentefrit,  
881 P. Moens, A. Dimou, B. Van Den Bossche, F. De Turck, S. Van  
882 Hoecke, F. Ongena, Flags: A methodology for adaptive anomaly  
883 detection and root cause analysis on sensor data streams by fusing  
884 expert knowledge with machine learning, Future Generation Computer  
885 Systems 116 (2021) 30–48. URL: <https://www.sciencedirect.com/science/article/pii/S0167739X20329927>. doi:<https://doi.org/10.1016/j.future.2020.10.015>.
- 888 T. Stauffer, D. Chastain-Knight, Do not let your safe operating limits leave you s-o-l (out of luck), Process Safety Progress 40 (2021) e12163. URL: <https://aiche.onlinelibrary.wiley.com/doi/abs/10.1002/prs.12163>. doi:<https://doi.org/10.1002/prs.12163>. arXiv:<https://aiche.onlinelibrary.wiley.com/doi/pdf/10.1002/prs.12163>.
- 893 M. Amer, M. Goldstein, S. Abdennadher, Enhancing one-class support vector machines for unsupervised anomaly detection, in: Proceedings of the ACM SIGKDD Workshop on Outlier Detection and Description, ODD '13, Association for Computing Machinery, New York, NY, USA, 2013, pp. 8–15. URL: <https://doi.org/10.1145/2500853.2500857>. doi:10.1145/2500853.2500857.
- 899 B. Liu, Y. Xiao, P. S. Yu, L. Cao, Y. Zhang, Z. Hao, Uncertain one-class learning and concept summarization learning on uncertain data streams, IEEE Transactions on Knowledge and Data Engineering 26 (2014) 468–484. doi:10.1109/TKDE.2012.235.
- 903 B. Krawczyk, M. Woźniak, One-class classifiers with incremental learning and forgetting for data streams with concept drift, Soft Computing 19 (2015) 3387–3400. URL: <https://doi.org/10.1007/s00500-014-1492-5>. doi:10.1007/s00500-014-1492-5.
- 907 X. Miao, Y. Liu, H. Zhao, C. Li, Distributed online one-class support vector machine for anomaly detection over networks, IEEE Transactions on Cybernetics 49 (2019) 1475–1488. doi:10.1109/TCYB.2018.2804940.
- 910 Ö. Gözüaçık, F. Can, Concept learning using one-class classifiers for implicit drift detection in evolving data streams, Artificial Intelligence Review 54 (2021) 3725–3747. URL: <https://doi.org/10.1007/s10462-020-09939-x>. doi:10.1007/s10462-020-09939-x.

- 914 R. Wetzig, A. Gulenko, F. Schmidt, Unsupervised anomaly alerting for  
915 iot-gateway monitoring using adaptive thresholds and half-space trees,  
916 in: 2019 Sixth International Conference on Internet of Things: Systems,  
917 Management and Security (IOTSMS), 2019, pp. 161–168. doi:10.1109/  
918 IOTSMS48152.2019.8939201.
- 919 Y. Lyu, W. Li, Y. Wang, S. Sun, C. Wang, Rmhsforest: Relative mass  
920 and half-space tree based forest for anomaly detection, Chinese Journal  
921 of Electronics 29 (2020) 1093–1101. doi:<https://doi.org/10.1049/cje.2020.09.010>.
- 923 B. P. Welford, Note on a method for calculating corrected sums of squares  
924 and products, Technometrics 4 (1962) 419–420. doi:10.1080/00401706.  
925 1962.10490022.
- 926 S. Mishra, A. Datta-Gupta, Chapter 3 - distributions and models thereof, in:  
927 S. Mishra, A. Datta-Gupta (Eds.), Applied Statistical Modeling and Data  
928 Analytics, Elsevier, 2018, pp. 31–67. URL: <https://www.sciencedirect.com/science/article/pii/B9780128032794000031>. doi:<https://doi.org/10.1016/B978-0-12-803279-4.00003-1>.
- 931 A. Genz, Numerical computation of multivariate normal probabilities, Journal  
932 of Computational and Graphical Statistics 1 (2000). doi:10.1080/  
933 10618600.1992.10477010.
- 934 F. Iglesias Vázquez, A. Hartl, T. Zseby, A. Zimek, Anomaly detection in  
935 streaming data: A comparison and evaluation study, Expert Systems with  
936 Applications 233 (2023) 120994. URL: <https://www.sciencedirect.com/science/article/pii/S0957417423014963>. doi:<https://doi.org/10.1016/j.eswa.2023.120994>.
- 939 L. Ruff, J. R. Kauffmann, R. A. Vandermeulen, G. Montavon, W. Samek,  
940 M. Kloft, T. G. Dietterich, K.-R. Müller, A unifying review of deep and  
941 shallow anomaly detection, Proceedings of the IEEE 109 (2021) 756–795.  
942 doi:10.1109/JPROC.2021.3052449.
- 943 I. D. Katser, V. O. Kozitsin, Skoltech anomaly benchmark (skab),  
944 <https://www.kaggle.com/dsv/1693952>, 2020. doi:10.34740/KAGGLE/DSV/1693952.

- 946 J. Montiel, M. Halford, S. M. Mastelini, G. Bolmier, R. Sourty, R. Vaysse,  
947 A. Zouitine, H. M. Gomes, J. Read, T. Abdessalem, A. Bifet, River: ma-  
948 chine learning for streaming data in python, Journal of Machine Learning  
949 Research 22 (2021) 1–8. URL: <http://jmlr.org/papers/v22/20-1380.html>.
- 950
- 951 F. Nogueira, Bayesian Optimization: Open source constrained global op-  
952 timization tool for Python, 2014. URL: <https://github.com/fmfn/>  
953 BayesianOptimization.